

Embedded Discrete Fracture Networks to Analyze Groundwater Inflows during Tunnel Drilling

Redes de fracturas discretas embebidas para el análisis de infiltraciones de agua subterránea durante la excavación de túneles

Adriana Piña¹, Diego Cortés², Leonardo David Donado³, and Daniela Blessent⁴

ABSTRACT

Tunnels commonly go through fracture zones, which are analyzed as an equivalent porous medium with homogeneous permeability. However, this is a rough simplification that overlooks the connection triggered by underground works in fractured massifs. This study introduces the use of synthetic discrete fracture networks (DFN) to analyze groundwater inflows through tunnel excavation in a fractured zone while considering the daily advance of the drilling front. First, a hypothetical case with six different settings, varying fracture length and density, as well as aperture distribution, was analyzed. Each setting had about 100 realizations. DFN hydraulic properties were estimated and compared with previous DFN studies, displaying the same behavior even though the magnitude of the estimated parameters differed. As an application example, structural measurements of the Alaska fault zone in the La Línea massif (Colombia) were used to obtain the statistical parameters of fracture length and aperture distributions to generate the DFN. Five settings were built, obtaining measured and simulated groundwater inflows of the same order of magnitude. These results highlight the potential of synthetic discrete fracture networks to analyze the effects of tunnel construction on groundwater flow.

Keywords: discrete fracture networks, groundwater inflows, numerical modeling, tunnel

RESUMEN

Los túneles usualmente atraviesan zonas geológicamente fracturadas, que suelen ser analizadas como medios porosos equivalentes de permeabilidad homogénea. Sin embargo, esta es una simplificación que ignora las conexiones que generan las obras subterráneas en un macizo fracturado. En este trabajo se introduce el uso de redes de fracturas sintéticas (DFN) para analizar los flujos de agua subterránea generados por la perforación de túneles, considerando el avance diario en el frente de excavación. En primer lugar, se analizó un caso hipotético con seis configuraciones diferentes, variando la densidad y longitud de las fracturas, así como la distribución de aperturas. Cada configuración tenía alrededor de 100 realizaciones. Las propiedades hidráulicas de la DFN fueron estimadas y comparadas con estudios previos sobre DFNs, mostrando el mismo comportamiento aún cuando la magnitud de los parámetros estimados difería. Como ejemplo de aplicación, se usó con información estructural de la falla Alaska en el macizo de la Línea (Colombia), con el fin de obtener los parámetros estadísticos de las distribuciones de longitud y apertura de las fracturas para la generación de las DFNs. Se crearon cinco configuraciones, obteniendo caudales de infiltración medidos y simulados del mismo orden de magnitud. Estos resultados resaltan el potencial del uso de redes sintéticas de fracturas para analizar el efecto de la construcción de túneles en el flujo de agua subterránea.

Palabras clave: redes de fracturas discretas, flujo de agua subterránea, modelación numérica, túnel

Received: August 12th, 2020

Accepted: July 2nd, 2021

¹Agricultural Engineer, M.Sc., Ph.D., School of Engineering, Universidad Nacional de Colombia, Colombia. Postdoctoral Researcher and Lecturer at HYDS Research Group, Universidad Nacional de Colombia at Bogota. E-mail: appinaf@unal.edu.co

²BSc, Civil Engineer, School of Engineering, Universidad Nacional de Colombia at Bogota. E-mail: diacortesra@unal.edu.co

³Civil Engineer, M.Sc., Ph.D. Affiliation: Full Professor at HYDS Research Group, Universidad Nacional de Colombia at Bogota. E-mail: lddonadog@unal.edu.co

⁴Environmental Engineer, M.Sc., Ph.D. Affiliation: Ph.D., Assistant Professor, Universidad de Medellín, Colombia, Colombia. E-mail: dblessent@udem.edu.co

How to cite: Piña, A., Cortés, D., Donado, L. D., and Blessent, D. (2022). Embedded Discrete Fracture Networks to Analyze Groundwater Inflows during Tunnel Drilling. *Ingeniería e Investigación*, 42(1), e89889. [10.15446/ing.investig.v42n1.89889](https://doi.org/10.15446/ing.investig.v42n1.89889)



Attribution 4.0 International (CC BY 4.0) Share - Adapt

Introduction

Fractured media refers to low permeability matrix rocks that may acquire moderate to good permeability thanks to fractures (Singhal and Gupta, 2010). There, underground projects for groundwater supply, waste disposal, or infrastructures are built up (Evans *et al.*, 2001; Singhal and Gupta, 2010), thus affecting the surrounding surface water sources and groundwater bodies. Some of the reported effects of tunnels are groundwater inflows during and after their construction (Celico *et al.*, 2005; Perrochet and Dematteis, 2007), groundwater and surface water level drawdown, (Molinero *et al.*, 2002; Maréchal and Etcheverry, 2003; Vincenzi *et al.*, 2009; Font-Capóet *et al.*, 2011), the triggering of preferential flow paths (Evans *et al.*, 2001), and rock deformations and instabilities (Preisig *et al.*, 2014; Shen *et al.*, 2014; Loew *et al.*, 2015; Valenzuela *et al.*, 2015).

Different modeling approaches have been implemented to assess the impact of underground projects both in the transient and steady state. In the steady state analysis, long term effects are studied, whereas in the transient state, the effects during the construction process are analyzed until a new steady state condition is reached (Celico *et al.*, 2005). Some analytical formulations based on the equivalent porous media (EPM) approach have been developed for steady state conditions and homogeneous materials (Goodman *et al.*, 1965; Heuer, 1995; Karlsrud, 2001; El Tani, 2003), and some have been extended to the transient-state. Perrochet (2005) evaluates the transient drilling speed-dependent discharge rates using a convolution integral, and extensions to the heterogeneous media have been proposed by Perrochet and Dematteis (2007) and Maréchal *et al.* (2014). Previous approaches do not consider the effect of the excavation-induced drawdown leading to over/underestimated groundwater inflows. For this reason, some authors have proposed analytical or semianalytical approaches to predict the height of lowered water level under the steady (Su *et al.*, 2017) and the transient states (Liu *et al.*, 2017), thus providing a better prediction of tunnel inflows.

Since most groundwater inflows are recorded in fault zones (Attanayake and Waterman, 2006; Perrochet and Dematteis, 2007; Yang *et al.*, 2009; UNAL, 2010; Moon and Fernandez, 2010; Zarei *et al.*, 2011; Loew *et al.*, 2015), fractures have been represented within heterogeneous media as more permeable areas with EPM approaches (Perrochet and Dematteis, 2007; Maréchal *et al.*, 2014; Preisig, 2013). This conceptualization has been extended to numerical modeling in order to predict groundwater inflow into tunnels (Maréchal *et al.*, 1999; Hu and Chen, 2008; Yang *et al.*, 2009; Butscher *et al.*, 2011; Chiu and Chia, 2012; Butscher, 2012; Xia *et al.*, 2018; Golian *et al.*, 2018; Nikvar Hassani *et al.*, 2018).

Even though the EPM approach allows the use of the above-mentioned analyses while the characterization of individual fractures, the complexity of the fractured media could be better represented by discrete fracture networks (DFN), where hydraulic behavior is controlled by their geometry (*i.e.*, aperture, length, density, and orientation distributions) (Adler *et al.*, 2012).

The inclusion of individual fractures or fracture networks in numerical modeling demands higher computational efforts to solve the problem. Nevertheless, some authors have included fractures on their analyses while accounting for the water management in tunnels (Molinero *et al.*, 2002; Lee *et al.*, 2006; Hawkins *et al.*, 2011; Hokr *et al.*, 2012, 2016; Farhadian *et al.*, 2016). Recently, Wang and Cai (2020) proposed a DFN-DEM multi-scale approach for modeling excavation responses in jointed rock masses for settlement purposes. However, the use of synthetic DFNs to estimate groundwater inflows into tunnels or underground works under a transient state has not been reported. In this study, we propose a numerical model to analyze the temporal evolution of groundwater inflows (hydrograph) during the construction of underground works in a fractured massif with a low permeability matrix. The novelty of this work is that

its conceptual model is based on a hybrid model with a DFN embedded on a low-permeability, continuous porous media. The generation of the synthetic DFN was carried out using the probabilistic functions of (i) frequency, (ii) length, (iii) aperture, and (iv) dip of the fractures. The groundwater flow model is bounded with a time-varying atmospheric pressure, which is activated according to a typical drilling speed of 2 m/d (Perrochet and Dematteis, 2007).

To show the capabilities of the proposed model, two types of simulation were performed. The first one is a hypothetical case with a randomly generated fracture network where the numerical model is tested. The second one consists of an embedded synthetic discrete fracture network (DFN) that is generated based on outcrop field data with information from surveys on La Línea massif in the Colombian Andes. The former only gives us information on the numerical performance of the groundwater model, whereas the second model is compared to the groundwater inflows recorded during the drilling of the La Línea tunnel (Colombia).

Methodology

The release of energy above the plastic limit fractures the rock Escobar, 2017, thus generating faulted planes that provide preferential flow paths through the massif rock (Leung and Zimmerman, 2012), which enhances the permeability of the media. Fractures are characterized by their length, surface roughness, aperture, fracture dead-end, and intersections (Adler *et al.*, 2012). These geological measurements are used to estimate hydraulic parameters (Liu *et al.*, 2016) by using frequency distributions such as the power law, lognormal, or exponential functions.

Fracture lengths have shown power-law distributions to have the greatest physical significance (Bonnet *et al.*, 2001) and ubiquitously describe scaling properties (Davy *et al.*, 2010). However, in nature, the frequency of fracture lengths displays *log-normal* (Equation (1)) or *exponential* distributions (Equation (2)) as result of the truncation effect induced by the sampling size, which limits the lower or upper boundary (Bonnet *et al.*, 2001).

$$n(l) = \frac{1}{l \cdot \sigma \sqrt{2\pi}} e^{-\frac{[\ln(l-\mu)]^2}{2\sigma^2}}, \quad (1)$$

$$n(l) = \frac{1}{\lambda} e^{-l/\lambda}, \quad (2)$$

where μ is the log-mean, σ is the log-standard-deviation, λ is a parameter of the exponential distribution, l is the fracture length, and $n(l)$ is the frequency distribution of fracture lengths.

Meanwhile, aperture distribution cannot be obtained easily from field measurements, which are uncertain because stresses change dramatically at depth (Liu *et al.*, 2016), and the weathering affects fracture appearance at outcrops. DFNs are realistic mappings of fracture geometries based on field observations via a stochastic representation of properties (Somogyvári *et al.*, 2017) such as fractures number, length, aperture, and dip. Their statistical parameters are the inputs

for several codes developed to generate and analyze DFNs, such as ADFNE (Fadakar Alghalandis, 2017), DFN WORKS (Hyman *et al.*, 2015), FracMan (Golder Associates Inc., 2018), and MoFrac (Mirarco, 2018). Nevertheless, these codes do not allow to simulate the advance in tunnel drilling processes, as it could be done using codes such as HydroGosSphere HGS (Aquanty Inc., 2013).

HGS is a 3D, fully integrated surface and subsurface flow simulator that is widely used in the analysis of groundwater issues (Aquanty Inc., 2013). It includes a Random Fracture Generator (RFG) that creates networks with random locations, lengths, and apertures by using any of the available probability distribution functions (PDF): exponential function for the aperture, exponential and lognormal functions for the fracture length, and a double-peaked Gaussian for the orientation. In this research, HGS and RFG were used to generate a synthetic DFN embedded on a very low permeability porous rock matrix.

In the following sections, we present the assumptions of the model components (mesh, DFN generation, definition of hydraulic parameters) and describe the initial and boundary conditions for the numerical simulations. All these components are described for both hypothetical and synthetic cases.

Mesh generation

The accuracy of groundwater models is affected by numerical errors or instabilities that occur in all computational simulations due to aspects such as grid spacing (Woods *et al.*, 2003; Anderson *et al.*, 2015). To ensure numerical stability in the modeling process, multiple preliminary simulations were performed, varying the number of fractures, block size, and grid spacing. Different block sizes were tested according to the width of the fault zones in the La Línea tunnel, which varies approximately from 20 m to 400 m, as well as to the total length of tunnel (8 600 m). Block size and grid spacing were identified as the most important aspects to guarantee a successful run, the availability of computational requirements, and a moderate simulation time. As result, a synthetic block of 400 m in length and height, 200 m in depth (which could be a representative volume for the La Gata, Alaska, or Cristalina fault zones in the La Línea massif), and mesh spacing varying from 1 to 80 m were chosen. In the middle of the block, the mesh was refined to simulate a tunnel with a radius of 2,5 m. That position was chosen to avoid boundary disturbances and aimed for symmetrical conditions. Mesh spacing limits the shortest fractures, while the model size limits the longest fractures. Using this scheme, each groundwater flow simulation took about 60 minutes using an Intel Xeon (@ 3.30GHz) and 32 GB RAM.

Synthetic DFN generation

RFG was used to create a DFN based on the statistical parameters of length, aperture, orientation, and number of fracture distributions. Fractures were randomly distributed in the porous media using a seed that can be changed to

allow the generation of an infinite number of different DFN with the same PDF for each fracture parameter. The resulting three-dimensional model is made of orthogonal blocks, where fractures are superposed as 2D elements to the sides of the 3D blocks, so that the fracture nodes coincide with those of the porous rock. The grid has to be thin enough to allow the creation of the fracture network. Nevertheless, extremely thin grids increase the number of elements and computation times.

A hundred DFN realizations for different configurations or settings were performed by varying density (expressed as the number of fractures generated) and fracture length parameter distributions (Equations (1) and (2)), while length distribution, grid, model dimensions, and hydraulic parameters were kept constant. However, some realizations could not be completed because of numerical instabilities.

DFN hydraulic properties

The hydraulic properties were used as indicators of DFN connectivity. Here, we considered the hydraulic conductivity of each fracture, K_f , the permeability of the fracture network (K_{DFN}), the volumetric fracture density (P_{32}), and the equivalent permeability (K_{EPM}) associated to the DFN mean flow (Q_{DFN}).

HGS estimates K_f by following the cubic law as $K(f) = \frac{gw_f^2}{12\nu}$, where $g[L/T^2]$ is gravity acceleration, $w_f[L]$, is the aperture, and $\nu[M/(L-T)]$ is the kinematic viscosity (Aquanty Inc., 2013). Thus, the permeability of the fracture network, K_{DFN} , was evaluated as the geometric mean of the K_f (de Dreuzy, 2001a). The volumetric fracture density, P_{32} , or the persistence of the fractures area (2D) per unit volume (3D), is expressed as $P_{32} = \frac{1}{V} \sum_f A_f = \frac{1}{V} \sum_f l_f \cdot b$, where V is the volume of model, A_f is the area of the fracture f , l_f is the length, and b the width of the model.

As each setting had as many hydrographs as completed simulations, an equivalent DFN hydrograph (Q_{DFN}) was calculated: $Q_{DFN} = \sum Q_{DFNi}/N$, where N is the number of completed i synthetic generations. Then, an equivalent porous media permeability (K_{EPM}) for each setting was calibrated based on 200 realizations in a homogeneous media configuration (EPM), where K was varied; specific storage, S_s , remained constant as the assigned value of the matrix domain in the DFN approach. In this way, a set of 200 EPM hydrographs Q_{EPM} were obtained, and Q_{DFN} was fitted to the set of Q_{EPM} using the Nash-Sutcliffe coefficient (NSE = $\left[1 - \frac{\sum (Q_{obs} - Q_{sim})^2}{\sum (Q_{obs} - Q_{obs})^2}\right]$; NSE values close to unity indicate good model performance) as the metric to select the K_{EPM} .

Hydraulic properties of the matrix

The matrix was considered as a very low permeable medium with a hydraulic conductivity (K) of 1×10^{-4} m/d, specific storage (S_s) equal to 5×10^{-4} , and porosity (η) equal to 4×10^{-3} (Singhal and Gupta, 2010).

Initial and boundary and conditions

An initial condition of head equal to topography is assigned to the entire domain. No flow conditions are assigned to the bottom and lateral faces of the cubic domain, considering the following assumptions specifically for the La Línea massif : i) preferential radial flow toward the tunnel (Preisig, 2013); ii) there are no significant regional flows, as the tunnel is located in the upper watershed; and iii) very low permeabilities of the crystalline rocks (IRENA, 2010; UNAL, 2015). These assumptions may be rejected due to possible connections with larger faults. However, it is an open issue when working with fractures and the consequent truncation effect due to the scale of the observation window.

A nodal flux of $1 \times 10^{-10} \text{ m}^3/\text{d}$ is assigned to the top face as an arbitrary recharge condition, in order to avoid a constant drawdown. The tunnel is simulated with a mobile boundary condition along the x -axis, in the middle of the $y - z$ plane. The advance of the tunnel drilling is simulated by assigning an atmospheric pressure at an excavation rate of 2 m/d (typical value for tunnel excavation rates (Perrochet and Dematteis, 2007; IRENA, 2007)). Tunnel excavation is completed in 200 days, and the recession flow is observed until 1 000 days.

Test cases

Two example cases were investigated using synthetic DFN in the analysis of groundwater inflows into a tunnel. The first case was a hypothetical block to test the performance of the numerical modeling. The second case was based on outcrop field data from the La Línea massif and the recorded groundwater inflows of the Alaska fault zone during the drilling of the La Línea tunnel.

Hypothetical case

In this case, the behavior of the hydrographs was analyzed by varying the fracture length, aperture, and density distributions. Six settings were built (each one with 100 realizations). The fracture length frequency was assumed to follow a log-normal distribution with $\mu = -4.5 \text{ m}$ and $\sigma = 3.4 \text{ m}$, whereas the exponential distribution was used for the fracture apertures. The fracture density or number of fractures was randomly assigned. Settings S1, S3, and S4 have the same density but their exponent λ varies from 8 000 to 10 000, while, in settings S2, S5, and S6 the exponent λ is kept constant (it is equal to 9 000). The parameters for each setting are displayed in Table 1.

The Alaska fault zone

As an application example, and based on the results from the hypothetical case, the Alaska fault zone was analyzed using five different settings, where fracture density was varied, and fracture length followed the statistical distribution of the La Línea massif.

The Alaska fault is located in the La Línea massif and is crossed by the drilling of two tunnels (Figure 1). These tunnels belong to an important roadway project in the Colombian Andes.

Table 1. Parameters for each configuration and number of completed generations for each setting

Setting	Number of fractures	λ	Completed realizations
S1	700	9 000	64
S2	350	9 000	77
S3	700	8 000	67
S4	700	10 000	48
S5	525	9 000	70
S6	175	9 000	90

Source: Authors

Their mean length is 8 600 m, the elevation at the East entrance is 2 434 m.a.s.l., 2 553 m.a.s.l. in the West, and the maximum depth is 800 m. The massif is formed by the Quebradagrande complex, the Cajamarca complex, and an andesitic porphyry. These geological formations are highly fractured and formed by igneous and metamorphic rocks with a complex structural geology (IRENA, 2007; UNAL, 2010). During the drilling process, important groundwater inflows were recorded, especially in fault zones (IRENA, 2007; UNAL, 2010). The Alaska fault zone is located in shales of the volcanic member of the Quebradagrande complex, Kv, as shown in Figure 1. The mean depth of the tunnel in the zone is 400 m.

When a tunnel is being drilled, there is a flow peak as the drilling front disturbs the rock followed by the recession flow, which diminishes or disappears depending on the hydrogeological conditions. In this way, the total amount of water drained by a tunnel is the convolution of each individual hydrograph. In the La Línea tunnel, the accumulated groundwater inflows were measured daily at each entrance of the tunnel (IRENA, 2007). However, there is no information on the real infiltration rates in specific zones. Hence, based on the average of 100 numerical simulations using an EPM approach, the recession flow of the first 1 000 m of tunnel is obtained and then removed from the accumulated data. Figure 2 displays the inflows recorded at the western entrance and the progression in the drilling front (IRENA, 2007); the hydrograph of the infiltrated water in the Alaska fault zone (inner box in Figure 2) was built subtracting the aforementioned recession or base flow (gray line). There, the drilling process took about 200 days, and about 40 l/s were recorded.

Fracture length distribution: The statistical parameters of the fracture lengths are obtained from structural maps at local and regional scale (10 000 m and 65 000 m, respectively) (Figure 1), considering that just few and small outcrops (less than 30 m) are found as consequence of the dense vegetation in the area.

Finding the best statistical distribution governing a dataset is of critical importance when predicting the tendency of fracture attributes (Rizzo *et al.*, 2017). The information criterion approach is implemented using the Akaike Information Criterion AIC (Akaike, 1974), the corrected AICc (Cavanaugh, 1997), the Bayesian Information Criteria BIC (Schwarz, 1978), and the KIC (Kashyap, 1982). Then, the estimation of the

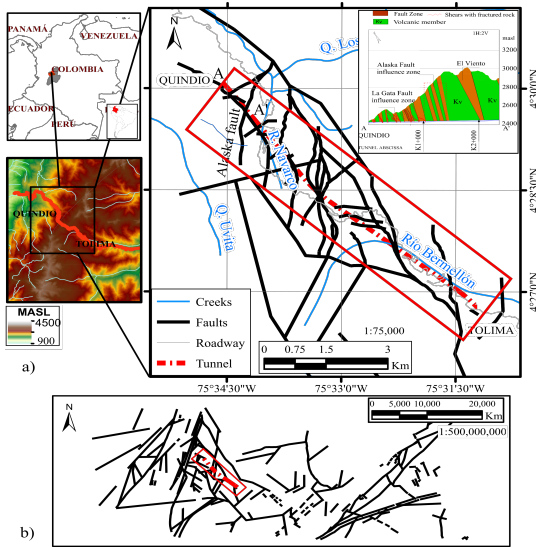


Figure 1. Geographical location of the La Lánea tunnel: a) Location of the Alaska fault and fractures at a local scale (10 000 m); and b) fractures at a regional scale (50 000 m).
Source: Authors

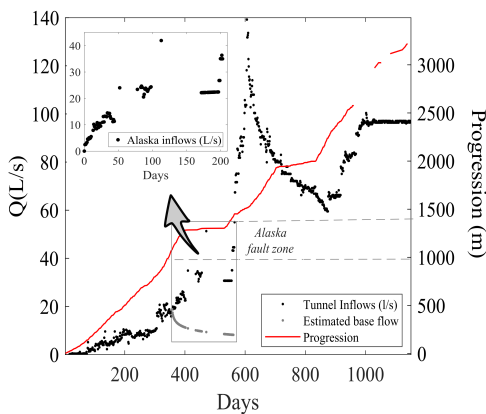


Figure 2. Daily groundwater inflows (black dots) and tunnel progression (red line); base flow (gray dots) was removed from accumulated hydrograph to obtain the Alaska inflows shown in the inner box (2007).
Source: Authors

posterior model weight (for AIC and AICc) or posterior model probability (for BIC and KIC) is implemented, as described in detail by Ye *et al.* (2008) and Siena *et al.* (2017). Fracture length was fitted to five probability density functions (normal, exponential, lognormal, gamma, and General Extreme Value-GEV) using the Maximum Likelihood Estimator approach. The four information criteria indicate the best fit for the exponential distribution with the lowest values. The same result is obtained by the posterior model weight or posterior model probability (showing the higher values) using the AIC, AICc, and BIC (Table 2). However, the KIC posterior probability is better for the GEV distribution, as it discriminates the models on the quality of the model parameter estimates (Siena *et al.*, 2017). Therefore, the exponential distribution is selected for the DFN generations of the Alaska fault zone with $\lambda = 3,16 \times 10^3$ m. The data fit

is shown in Figure 3.

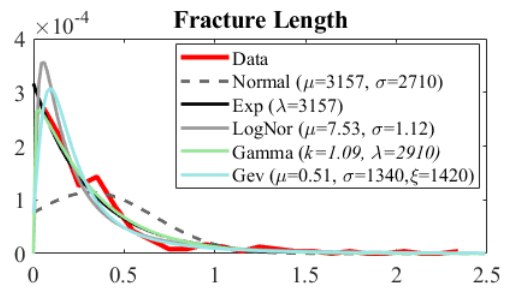


Figure 3. Probability density functions for fracture length in Alaska fault zone in the La Lánea tunnel.
Source: Authors

Table 2. Posterior weights/model probability of the five analytical models evaluated for the model identification criterion

Criteria	Normal	Exponential	Lognormal	Gamma	GEV
AIC	0	34,00	16,99	30,83	18,17
BIC	0	44,24	15,62	28,34	11,80
AICc	0	34,00	16,99	30,83	18,17
KIC	0	29,65	3,14	22,51	44,7

Source: Authors

An example of the synthetic DFN generated using the lognormal (hypothetical case) and the exponential distribution for the fracture length with the same number of fractures is shown in Figure 4.

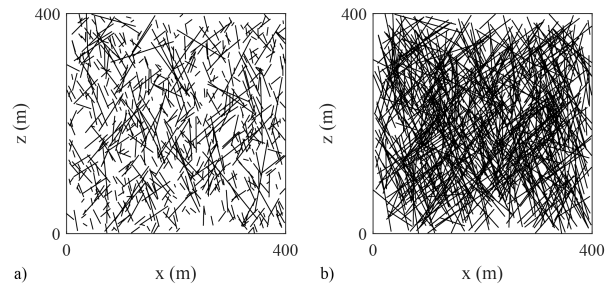


Figure 4. Example of the generated DFN: (a) hypothetical case and (b) application example for the Alaska fault zone.
Source: Authors

Fracture aperture: Regarding the aperture information, it was not possible to obtain aperture measurements within the massif, or any information to estimate a real value. Mean aperture measurements on surface were 1,5 mm, the minimum was 0 mm, and the maximum was 32 mm (Hernandez and Kammer, 2016). These values are extremely high, as result of the weathering of the outcrops. They do not even allow running the model because of numerical convergence issues. However, preliminary tests showed that the default HGS aperture distribution approach worked fine. Consequently, the aperture generation range was kept between $25 \mu\text{m}$ and $3,2 \times 10^2 \mu\text{m}$, and λ equal to $9,0 \times 10^3$ for the exponential distribution (Equation 2).

Results

Hypothetical case

Figure 5a displays the hydrographs for each completed generation in S1, the estimated mean, and the standard deviation (σ). Peak groundwater inflows vary between 28 and 52 L/s, and the recession flows are less spread than those observed for early times. In the estimation of K_{EPM} , it is important to consider that HGS changes the time step to optimize CPU requirements; when the simulated variable shows large variations, time steps are smaller. On the contrary, if no sensible variation is simulated, the time steps increase. After 200 days, when excavation is finished, and hydraulic heads do not vary significantly, the time step increases, and only ten values are generated in the remaining 800 days. For this reason, when the NASH coefficient is calculated, differences between Q_{EPM} and Q_{DFN} in the recession zone of the hydrograph are not so relevant, and the NASH coefficient values are close to one.

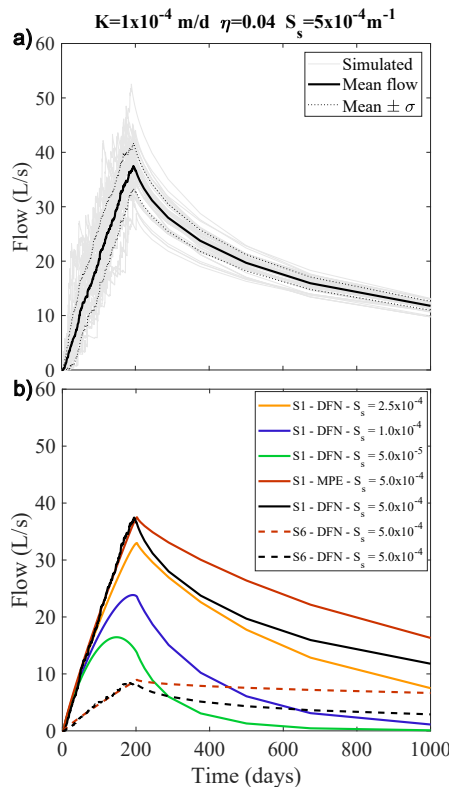


Figure 5. Hydrographs of the simulated groundwater inflows for DFN generations: a) setting 1 (S1); b) mean flow obtained using the DFN and EPM approaches using different fracture densities (settings S1 and S6) and DFN approach for S1, showing the influence of S_s (m^{-1}) in the simulated flows.

Source: Authors

Table 3 contains K_{EPM} , NASH, and K_{DFN} for each setting. K_{EPM} varies between 8×10^{-3} and 4×10^{-2} m/d, while K_{DFN} ranges from 5×10^2 to 6×10^2 m/d. The difference between both approaches (K_{EPM} and K_{DFN}) exceeds 5 orders of magnitude. Therefore, the values are not comparable, and the assumption of an equivalent permeability of the media,

estimated as K_{DFN} and proposed by de Dreuzy *et al.* (2001b), does not work in this study. It may be associated to the matrix of low permeability and P_{32} below 1 used in this research. Consequently, the effects of matrix permeability and fracture density should be taken into account for future modeling and analysis.

Table 3. Equivalent and geometric mean permeability of fractures for each setting

Setting	K_{EPM} (m/d)	NASH	K_{DFN} (m/d)
S1	$4,03 \times 10^{-2}$	0,99	$5,63 \times 10^2$
S2	$1,97 \times 10^{-2}$	0,96	$5,63 \times 10^2$
S3	$4,03 \times 10^{-2}$	0,99	$5,17 \times 10^2$
S4	$4,36 \times 10^{-2}$	0,99	$6,15 \times 10^2$
S5	$3,00 \times 10^{-2}$	0,98	$5,63 \times 10^2$
S6	$8,00 \times 10^{-3}$	0,97	$5,60 \times 10^2$

Source: Authors

Figure 5b displays the calculated Q_{DFN} for different fracture densities in settings S1 and S6, and Q_{EPM} , showing how flow increases as the number of fractures does. The excavation phase shows a good fit between EPM and DFN (until 200 days). However, the tail of the hydrograph is overestimated by the EPM approach, which leads us to perform a sensitivity analysis of the S_s for S1, showing how the peak and the recession flow decrease as a function of S_s .

Based on the obtained results, DFN hydraulic parameters (introduced in the section named after them) were estimated and compared with previous studies (de Dreuzy *et al.*, 2001b; Maillot *et al.*, 2016) in order to validate the behavior of the generated DFN. Figure 6 displays the relationship between permeability and P_{32} for the settings where only the fracture density changes (S1, S2, S5, and S6). A linear relationship between the K_{EPM} and the P_{32} is observed, as found by Maillot *et al.* (2016), but in a lower density range, considering that the estimated P_{32} for the analyzed configuration is below 1.

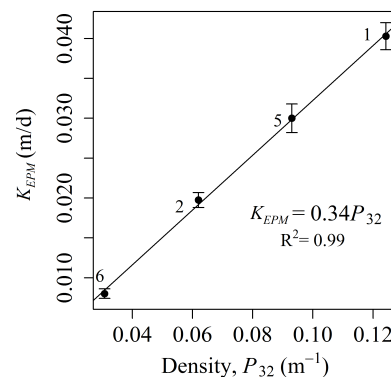


Figure 6. Linear relationship between permeability and fracture density P_{32} , displaying the 95% confidence interval bars of the K_{EPM} (tags indicate the setting number).

Source: Authors

The Alaska fault zone

In this subsection, the results of a more complex fracture network (Figure 1) are presented. The statistical properties for the fracture lengths of the maps (Figure 2) were taken to configure the DFN generation, and the fracture density was varied from 55 to 700 fractures, as indicated in Table 4. As the density changes, connectivity does as well, and, consequently, K_{EPM} (Table 4). However, in this application, the linear relationship observed in the synthetic example (Figure 6) and reported by Maillot *et al.* (2016) is not preserved for the most dense setting (700 fractures), as shown in Figure 7. It is probably a truncation effect caused by the lower number of numerically successful runs (55 of 100 simulations) caused by the difficulty to locate a higher number of fractures in the same domain size and mesh distribution.

Finally, by visual inspection, the synthetic DFN with about 400 fractures generates hydrographs that show a good agreement with the measured inflows in the first 100 days (Figure 8). Unfortunately, there are no records for 60 days, probably as a result of construction problems due to rock quality and the presence of water, which caused the drilling advance to be almost stopped. This would explain the decrease in the flows from 180 to 200 days, followed by a sudden increase as tunnel blasting was resumed. This kind of situation during construction activities is the greatest limitation in the acquisition of information for every geological unit, in addition to the complexity involved in the behavior of the recession flow.

Table 4. Density and K_{EPM} for five settings with different number of fractures implemented for the Alaska fault zone

Number of fractures	P_{32} (m^{-1})	(m/d)	Completed generations
55	$3,20 \times 10^{-2}$	$5,92 \times 10^{-3}$	95
188	$1,10 \times 10^{-1}$	$2,69 \times 10^{-2}$	86
400	$2,37 \times 10^{-1}$	$5,43 \times 10^{-2}$	56
500	$3,01 \times 10^{-1}$	$6,70 \times 10^{-2}$	62
700	$4,10 \times 10^{-1}$	$7,79 \times 10^{-2}$	62

Source: Authors

Discussion

The accurate distribution of fractures in a rock massif is almost impossible to know. Synthetic DFN generations can be used as a tool to model the effects caused by tunnel drilling through fault zones, considering the daily advance in the perforation work.

Figures 6 and 7 show how geological media permeability is heavily dependent on DFN density, P_{32} . However, for the application example of the Alaska fault zone, a perfectly linear relationship is not observed. This may be associated to a truncation effect in the fractures.

The behavior of high-density DFNs in a very low permeability matrix has important characteristics: groundwater must flow through fractures, so that the DFN has to be connected in order to contribute to groundwater circulation. In the porous

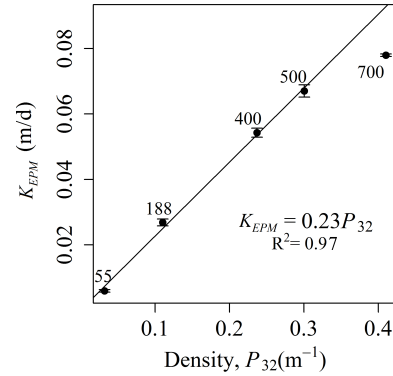


Figure 7. Relationship between permeability and fracture density P_{32} for the Alaska fault zone, displaying the 95% confidence interval bars of the K_{EPM} (tags indicate the number of fractures in each setting).

Source: Authors

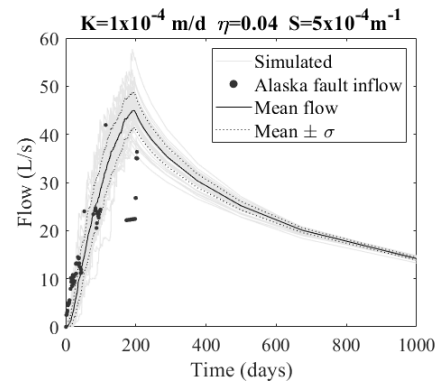


Figure 8. Groundwater inflows simulated for the 400-fracture setting and measured flow in Alaska fault zone (black dots).

Source: Authors

matrix, unconnected fractures take part in groundwater flow through the matrix, and their influence is especially notorious during tunnel excavation. When drilling crosses a fracture, water flows freely as a function of its aperture, and a new connection is generated through the system. Then, a drilled porous matrix gradually releases the water stored in the massif. This explains the fact that EPM overestimates late inflows when permeability is adjusted.

The importance of the S_s in the estimated groundwater inflows for the recession period is evidenced. However, as there are no measured data for this period to fit any parameter, only synthetic data are compared. In this way, the closest behavior between a DFN realization and an EPM was obtained using S_s equal to $2,5 \times 10^{-4} m^{-1}$, which is within the range of the reported specific storage values for crystalline rocks (Hartley and Joyce, 2013).

Conclusions

This work highlights the possibility of implementing synthetic DFNs to analyze the effects of the advance of tunnels excavation in fractured zones. The results show that, based on

the statistical parameters of the structural geology of a massif (*i.e.*, fracture length and aperture measured in geological maps or outcrops), synthetic DFNs can reproduce groundwater inflows of the same order of magnitude than those measured in the Alaska fault zone in the La Línea tunnel, Colombia. This is an outstanding finding of this research, as the results were compared with real data, which has never been reported before. Unfortunately, there are no available measured data of the hydrograph at late times for this specific zone, so Ss estimation is an open issue. As input information of a fracture network is scarce, uncertainty is high. However, it can be established that fracture density, P_{32} , is the parameter that most influences the estimated EPM permeability for the conditions of this study, which is in agreement with Maillot *et al.* (2016). The relationship between P_{32} and equivalent permeability is heavily influenced by the fracture length distribution. Thus, a linear performance cannot be always supposed, probably because of the truncation effect caused by the size of the synthetic model.

Acknowledgements

The authors would like to thank Professor Rene Therrien (Université Laval) for supplying the HGS license, as well as Colciencias-Universidad Nacional de Colombia for the Ph.D. Financing Program 617-2014. This research was also funded by Instituto Nacional de Vías (INVIAS).

References

- Adler, P., Thovert, J.-F., and Mourzenko, V. (2012). *Fractured Porous Media* (1st ed.). Oxford University Press. 10.1061/10.1093/acprof:oso/9780199666515.003.0001
- Akaike, H. (1974). A New Look at the Statistical Model Identification. *IEEE Transactions on Automatic Control*, 19(6), 716-723. 10.1061/10.1109/TAC.1974.1100705
- Anderson, M., Woessner, W., and Hunt, R. (2015). *Applied Groundwater Modeling Simulation of Flow and Advective Transport* (2nd ed.). Elsevier.
- Aquanty Inc. (2013). *HydroGeoSphere user manual*. <https://www.aquanty.com/hydrogeosphere>
- Attanayake, P. M. and Waterman, M. K. (2006). Identifying environmental impacts of underground construction. *Hydrogeology Journal*, 14, 1160-1170. 10.1061/10.1007/s10040-006-0037-0
- Bonnet, E., Bour, O., Odling, N. E., Davy, P., Main, I., Cowie, P., and Berkowitz, B. (2001). Scaling of fracture systems in geological media. *Reviews of Geophysics*, 39(3), 347-383. 10.1061/10.1029/1999RG000074
- Butscher, C., Einstein, H. H., and Huggenberger, P. (2011). Effects of tunneling on groundwater flow and swelling of clay-sulfate rocks. *Water Resources Research*, 47(11), 1-17. 10.1061/10.1029/2011WR011023
- Butscher, C. (2012). Steady-state groundwater inflow into a circular tunnel. *Tunnelling and Underground Space Technology*, 32, 158-167. 10.1061/10.1016/j.tust.2012.06.007
- Cavanaugh, J. E. (1997). Unifying the derivations for the Akaike and corrected Akaike information criteria. *Statistics & Probability Letters*, 33(2), 201-208. 10.1061/10.1016/S0167-7152(96)00128-9
- Chiu, Y.-C. and Chia, Y. (2012). The impact of groundwater discharge to the Hsueh-Shan tunnel on the water resources in northern Taiwan. *Hydrogeology Journal*, 20, 1599-1611. 10.1061/10.1007/s10040-012-0895-6
- Celico, P., Fabbrocino, S., Petitta, M., and Tallini, M. (2005). Hydrogeological impact of the Gran Sasso motor-way tunnels (Central Italy). *Giornale di Geologia Applicata*, 1, 157-165.
- Davy, P., Le Goc, R., Darcel, C., Bour, O., de Dreuzy, J.-R., and Munier, R. (2010). A likely universal model of fracture scaling and its consequence for crustal hydromechanics. *Journal of Geophysical Research: Solid Earth*, 115(B10), 1-13. 10.1061/10.1029/2009JB007043
- de Dreuzy, J.-R., Davy, P., and Bour, O. (2001a). Hydraulic properties of two-dimensional random fracture networks following a power law length distribution: 1. Effective connectivity. *Water Resources Research*, 37(8), 2065-2078. 10.1061/10.1029/2001WR900011
- de Dreuzy, J.-R., Davy, P., and Bour, O. (2001b). Hydraulic properties of two-dimensional random fracture networks following power law distributions of length and aperture. *Water Resources Research*, 38(2), 12-1-12-9. 10.1061/10.1029/2001WR001009
- El Tani, M. (2003). Circular tunnel in a semi-infinite aquifer. *Tunnelling and Underground Space Technology*, 18(1), 49-55. 10.1061/10.1016/S0886-7798(02)00102-5
- Escobar, G. (2017). *Manual de geología para ingenieros*. Universidad Nacional de Colombia, Sede Manizales. <https://repositorio.unal.edu.co/handle/unal/3145>
- Evans, D. D., Nicholson, T. J., and Rasmussen, T. C. (Eds.) (2001). *Flow and Transport Through Unsaturated Fractured Rock*. American Geophysical Union. 10.1061/10.1029/GM042
- Fadakar Alghalandis, Y. (2017). ADFNE: Open source software for discrete fracture network engineering, two and three dimensional applications. *Computers and Geosciences*, 102, 1-11. 10.1061/j.cageo.2017.02.002
- Farhadian, H., Katibeh, H., Huggenberger, P., and Butscher, C. (2016). Optimum model extent for numerical simulation of tunnel inflow in fractured rock. *Tunnelling and Underground Space Technology*, 60, 21-29. 10.1016/j.tust.2016.07.014
- Font-Capó, J., Vázquez-suñé, E., Carrera, J., and Martí, D. (2011). Groundwater in flow prediction in urban tunneling with a tunnel boring machine (TBM). *Engineering Geology*, 121(1-2), 46-54. 10.1016/j.enggeo.2011.04.012
- Golder Associates Inc. (2018) *FracMan*. <https://www.golder.com/fracman/>
- Golian, M., Teshnizi, E. S., and Nakhaei, M. (2018). Prediction of water inflow to mechanized tunnels during tunnel-boring-machine advance using numerical simulation. *Hydrogeology Journal*, 26, 2827-2851. 10.1007/s10040-018-1835-x

- Goodman, R., Moye, D., Schalkwyk, A., and Javandel, I. (1965). Groundwater inflows during tunnel driving. *Bulletin of the International Association of Geologists*, 2, 35-56.
- Hartley, L., and Joyce, S. (2013). Approaches and algorithms for groundwater flow modeling in support of site investigations and safety assessment of the Forsmark site, Sweden. *Journal of Hydrology*, 500, 200-216. 10.1016/j.jhydrol.2013.07.031
- Hawkins, I. R. and Swift, B. T., Hoch, a. R., and Wendling, J. (2011). Comparing flows to a tunnel for single porosity, double porosity and discrete fracture representations of the EDZ. *Physics and Chemistry of the Earth, Parts A/B/C*, 36(17-18), 1990-2002. 10.1016/j.pce.2011.07.029
- Hernández, F. and Kammer, A. (2016). *Caracterización estructural de los complejos Cajamarca y Quebradagrande en la zona del túnel de la línea, con implicaciones hidrogeológicas* [Undergraduate thesis].
- Heuer, R. (1995). Estimating rock-tunnel water inflow. In G. E. Williamson (Ed.) *Proceedings of the Rapid Excavation and Tunneling Conference* (pp. 41-60). SME.
- Hokr, M., Škarydová, I., and Frydrych, D. (2012). Modelling of tunnel inflow with combination of discrete fractures and continuum. *Computing and Visualization in Science*, 15, 21-28. 10.1007/s00791-013-0194-3
- Hokr, M., Shao, H., Gardner, W. P., Balvín, A., Kunz, H., Wang, Y., and Vencel, M. (2016). Real-case benchmark for flow and tracer transport in the fractured rock. *Environmental Earth Sciences*, 75(18), 1273. 10.1007/s12665-016-6061-z
- Hu, L. T. and Chen, C. X. (2008). Analytical methods for transient flow to a well in a confined- unconfined aquifer. *Ground Water*, 46(4), 642-646. 10.1111/j.1745-6584.2008.00436.x
- Hyman, J. D., Karra, S., Makedonska, N., Gable, C. W., Painter, S. L., and Viswanathan, H. S. (2015). DFN WORKS: A discrete fracture network framework for modeling subsurface flow and transport. *Computers and Geosciences*, 84, 10-19. 10.1016/j.cageo.2015.08.001
- IRENA (2007). *Estudios hidrogeológicos e hidrológicos en el área de influencia del túnel piloto de la línea, enmarcado dentro de la gestión ambiental*. IRENA.
- IRENA (2010). *Actualización a 2009 del modelo hidrogeológico del Túnel de la Línea*. INIVIAS - Ministerio del Transporte.
- Karlsruud, K. (2003). Water control when tunneling under urban areas in the Oslo region. *NFF publication*, 12, 27-33.
- Kashyap, R. L. (1982). Optimal Choice of AR and MA Parts in Autoregressive Moving Average Models. *IEEE Transactions on Pattern Analysis and Machine Intelligence, PAMI-4*(2), 99-104. 10.1109/TPAMI.1982.4767213
- Lee, H., Son, B., Kim, Y., and Jeon, S. (2006). Discrete fracture network and equivalent hydraulic conductivity for tunnel seepage analysis in rock mass. *Tunnelling and Underground Space Technology*, 21(3-4), 403. 10.1016/j.tust.2005.12.212
- Leung, C. T. O. and Zimmerman, R. W. (2012). Estimating the Hydraulic Conductivity of Two-Dimensional Fracture Networks Using Network Geometric Properties. *Transport in Porous Media*, 93, 777-797. 10.1007/s11242-012-9982-3
- Liu, R., Li, B., and Jiang, Y. (2016). A fractal model based on a new governing equation of fluid flow in fractures for characterizing hydraulic properties of rock fracture networks. *Computers and Geotechnics*, 75, 57-68. 10.1016/j.compgeo.2016.01.025
- Liu, R., Yu, L., Jiang, Y., Wang, Y., and Li, B. (2017). Recent developments on relationships between the equivalent permeability and fractal dimension of two-dimensional rock fracture networks. *Journal of Natural Gas Science and Engineering*, 45, 771-785. 10.1016/j.jngse.2017.06.013
- Loew, S., Lutzenkirchen, V., Hansmann, J., Ryf, A., and Guntli, P. (2015). Transient surface deformations caused by the Gotthard Base Tunnel. *International Journal of Rock Mechanics and Mining Sciences*, 75, 82-101. 10.1016/j.ijrmmms.2014.12.009
- Maillot, J., Davy, P., Le Goc, R., Darcel, C., and de Dreuzy, J.-R. (2016). Connectivity, permeability and channeling in randomly-distributed and kinematically-defined discrete fracture network models. *Water Resources Research*, 52(11), 613-615. 10.1002/2016WR018973
- Maréchal, J.-C., Perrochet, P., and Tacher, L. (1999). Long-term simulations of thermal and hydraulic characteristics in a mountain massif: The Mont Blanc case study, French and Italian Alps. *Hydrogeology Journal*, 7, 341-354. 10.1007/s100400050207
- Maréchal, J.-C. and Etcheverry, J. (2003). The use of 3H and 18O tracers to characterize water inflows in Alpine tunnels. *Applied Geochemistry*, 18(3), 339-351. 10.1016/S0883-2927(02)00101-4
- Maréchal, J.-C., Lanini, S., Aunay, B., and Perrochet, P. (2014). Analytical solution for modeling discharge into a tunnel drilled in a heterogeneous unconfined aquifer. *Ground Water*, 52(4), 597-605. 10.1111/gwat.12087
- Mirarco (2018). *MoFrac: Discrete fracture network modeling*. <https://mofrac.com>
- Molinero, J., Samper, J., and Juanes, R. (2002). Numerical modeling of the transient hydrogeological response produced by tunnel construction in fractured bedrocks. *Engineering Geology*, 64(4), 369-386. 10.1016/S0013-7952(01)00099-0
- Moon, J. and Fernandez, G. (2010) Effect of Excavation-Induced Groundwater Level Drawdown on Tunnel Inflow in a Jointed Rock Mass. *Engineering Geology*, 110(3-4), 33-42. 10.1016/j.enggeo.2009.09.002
- Nikvar Hassani, A., Farhadian, H., and Katibeh, H. (2018). A comparative study on evaluation of steady-state groundwater inflow into a circular shallow tunnel. *Tunnelling and Underground Space Technology*, 73, 15-25. 10.1016/j.tust.2017.11.019
- Perrochet, P. (2005). Confined flow into a tunnel during progressive drilling: An analytical solution. *Ground Water*, 43(6), 943-946. 10.1111/j.1745-6584.2005.00108.x

- Perrochet, P. and Dematteis, A. (2007). Modeling transient discharge into a tunnel drilled in a heterogeneous formation. *Ground Water*, 45(6), 786-790. 10.1111/j.1745-6584.2007.00355.x
- Preisig, G. (2013). Regional simulation of coupled hydromechanical processes in fractured and granular porous aquifer using effective stress-dependent parameters. [Doctoral thesis, University of Neuchâtel].
- Preisig, G., Dematteis, A., Torri, R., Monin, N., Milnes, E., and Perrochet, P. (2014). Modelling discharge rates and ground settlement induced by tunnel excavation. *Rock Mechanics and Rock Engineering*, 47, 869-884. 10.1007/s00603-012-0357-4
- Rizzo, R. E., Healy, D., and de Siena, L. (2017). Benefits of maximum likelihood estimators for fracture attribute analysis: Implications for permeability and up-scaling, *Journal of Structural Geology*, 95, 17-31. 10.1016/j.jsg.2016.12.005
- Schwarz, G. (1978). Estimating the Dimension of a Model. *The Annals of Statistics*, 6(2), 461-464. 10.1214/aos/1176344136
- Shen, S.-L., Wu, H.-N., Cui, Y.-J., and Yin, Z.-Y. (2014). Long-term settlement behaviour of metro tunnels in the soft deposits of Shanghai. *Tunnelling and Underground Space Technology*, 40, 309-323. 10.1016/j.tust.2013.10.013
- Siena, M., Riva, M., Giamberini, M., Gouze, P., and Guadagnini, A. (2017). Statistical modeling of gas-permeability spatial variability along a limestone core. *Spatial Statistics*, 34, 100249. 10.1016/j.spasta.2017.07.007
- Singhal, B. B. S. and Gupta, R. (2010). *Applied Hydrogeology of Fractured Rocks*. Springer. 10.1007/978-90-481-8799-7
- Somogyvári, M., Jalali, M., Jiménez-Parras, S., and Bayer, P. (2017). Synthetic fracture network characterization with transdimensional inversion. *Water Resources Research*, 53(6), 5104-5123. 10.1002/2016WR020293
- Su, K., Zhou, Y., Wu, H., Shi, C., and Zhou L. (2017). An Analytical Method for Groundwater Inflow into a Drained Circular Tunnel. *Ground Water*, 55(5), 1-10. 10.1111/gwat.12513
- Universidad Nacional de Colombia (UNAL) (2010). *Evaluación del impacto de la construcción de los túneles viales del Sumpaz y de La Línea en los hidrosistemas circunvecinos* [Doctoral thesis, Universidad Nacional de Colombia]. Grupo de Investigación en Ingeniería de Recursos Hídricos. <https://repositorio.unal.edu.co/handle/unal/68766>
- Universidad Nacional de Colombia (UNAL) (2015). *Informe Final Ensayos Hidráulicos Especiales en el Macizo Fracturado de La Línea*. Grupo de Investigación en Ingeniería de Recursos Hídricos, 2015.
- Valenzuela, P., Domínguez-Cuesta, M. J., Meléndez-Asensio, M. J., Jiménez-Sánchez, M., and de Santa María, J. A. S. (2015). Active sinkholes: A geomorphological impact of the Pajares Tunnels (Cantabrian Range, NW Spain). *Engineering Geology*, 196, 158-170. 10.1016/j.enggeo.2015.07.007
- Vincenzi, V., Gargini, A., and Goldscheider, N. (2009). Using tracer tests and hydrological observations to evaluate effects of tunnel drainage on groundwater and surface waters in the Northern Apennines (Italy). *Hydrogeology Journal*, 17, 135-150. 10.1007/s10040-008-0371-5
- Wang, X. and Cai, M. (2020). A DFN DEM Multi-scale Modeling Approach for Simulating Tunnel Excavation Response in Jointed Rock Masses. *Rock Mechanics and Rock Engineering*, 53, 1053-1077. 10.1007/s00603-019-01957-8
- Woods, J. A., Teubner, M. D., Simmons, C. T., Narayan, K. A. (2003). Numerical error in groundwater flow and solute transport simulation. *Water Resources Research*, 39(6). 10.1029/2001WR000586
- Xia, Q., Xu, M., Zhang, H., Zhang, Q. and Xiao, X. (2018). A dynamic modeling approach to simulate groundwater discharges into a tunnel from typical heterogeneous geological media during continuing excavation. *KSCCE Journal of Civil Engineering*, 22, 341-350. 10.1007/s12205-017-0668-9
- Yang, F.-R., Lee, C.-H., Kung, W.-J., and Yeh, H.-F. (2009). The impact of tunneling construction on the hydrogeological environment of "Tseng-Wen Reservoir Transbasin Diversion Project" in Taiwan. *Engineering Geology*, 103(1-2), 39-58. /10.1016/j.enggeo.2008.07.012
- Ye, M., Meyer, P. D., and Neuman, S. P. (2008). On model selection criteria in multimodel analysis. *Water Resources Research*, 44(3), 1-12. 10.1029/2008WR006803
- Zarei, H. R., Uromeihy, A., and Sharifzadeh, M. (2011). Evaluation of high local groundwater inflow to a rock tunnel by characterization of geological features. *Tunnelling and Underground Space Technology*, 26(2), 364-373. 10.1016/j.tust.2010.11.007